Changes in Hydrogen Bonding and Environment of Tryptophan Residues on Helix F of Bacteriorhodopsin during the Photocycle: A Time-Resolved Ultraviolet Resonance Raman Study

Shinji Hashimoto,*,‡ Masato Sasaki,§,|| Hideo Takeuchi,§ Richard Needleman,⊥ and Janos K. Lanyi#

Faculty of Science and Engineering, Tokyo University of Science, Yamaguchi, Daigaku Dori, Onoda 756-0884, Japan, Graduate School of Pharmaceutical Sciences, Tohoku University, Aobayama, Sendai 980-8578, Japan, Department of Biochemistry, Wayne State University, Detroit, Michigan 48201, and Department of Physiology and Biophysics, University of California, Irvine, California 92717

Received December 26, 2001; Revised Manuscript Received March 26, 2002

ABSTRACT: Protein structural changes during the photocycle of bacteriorhodopsin were examined by time-resolved ultraviolet resonance Raman (UVRR) spectroscopy. Most of the 244-nm UVRR difference signals of Trp were assigned to either Trp182 or Trp189 using the Trp182 → Phe and Trp189 → Phe mutants. The W17 mode of Trp182 shows a wavenumber downshift in the $M_1 \rightarrow M_2$ transition, indicating an increase in hydrogen bonding strength at the indole nitrogen. On the other hand, Trp189 shows Raman intensity increases of the W16 and W18 modes ascribable to an increased hydrophobic interaction. These observations suggest that the tilt of helix F, which ensures that reprotonation of the Schiff base is from the cytoplasmic side, occurs in the $M_1 \rightarrow M_2$ transition. In the $M_2 \rightarrow N$ transition, the environment of Trp189 returns to the initial state, whereas the hydrophobic interaction of Trp182 decreases drastically. The decrease in hydrophobic interaction of Trp182 in the N state suggests an invasion of water molecules that promote the proton transfer from Asp96 to the Schiff base. Structural reorganization of the protein after the tilt of helix F may be important for efficient reprotonation of the Schiff base.

Bacteriorhodopsin (BR),[1] a transmembrane protein of *Halobacterium salinarium*, utilizes light energy to transport protons across the cell membrane (*1*). BR consists of seven helices, A−G, with a chromophore, *all-trans*-retinal, covalently linked to Lys216 near the middle of helix G via a protonated Schiff base (*2*). Illumination of BR with visible light triggers isomerization of the retinal chromophore from all-trans to 13-cis, and the photoexcited protein relaxes to the initial light-adapted BR state via intermediates J, K, L, M, N, and O (*3*, *4*). During the photocycle, a proton is translocated from the cytoplasmic side to the extracellular side of the membrane (*1*). By combining diffraction data on the ground and photointermediate states with spectroscopic and mutational data, molecular models for the proton translocation across the cell membrane have been proposed (for recent reviews, see refs *5* and *6*).

According to a current model, the initial proton transport takes place from the interior to the extracellular side of BR in the transition from L to M. The protonated Schiff base in the interior loses its proton to anionic Asp85, and this induces displacement of the side chain of Arg82 toward the extracellular side, which subsequently results in a proton release to the extracellular medium from a site near the extracellular surface. The deprotonated Schiff base is reprotonated in the M → N transition by the protonated Asp96 located in the cytoplasmic half of BR. Asp96 then acquires a proton from the cytoplasmic medium, and the retinal reisomerizes to a twisted all-trans configuration in the N → O transition. In the last step of the O → BR transition, a proton is transferred from Asp85 to the proton release site, and the twisted retinal relaxes into the initial state. A key component in the transport is the switch of the proton path around the Schiff base from the extracellular side in the L−M phase to the cytoplasmic side in the M−N phase, which may involve changes in protein structure during the formation and decay of the M intermediate (*7*, *8*).

Changes in protein tertiary structure during the photocycle have been detected by diffraction and spectroscopic methods. Subramaniam et al. examined by electron diffraction the structure of a long-lived M intermediate of the D96G mutant (*9*), which was later shown to be in an N-like protein structure and named M_N (*10*). According to their result, the cytoplasmic end of helix F is shifted away from the center of the protein, and helix G becomes more ordered in the M_N state compared to the ground state. The tilt of helix F in the N protein structure was also suggested by electron and X-ray diffraction for the F219L (*11*, *12*) and F171C mutants (*13*), and is consistent with the result of a time-resolved electron paramagnetic resonance (EPR) study that the distances of the E−F interhelical loop from the A−B and

* To whom correspondence should be addressed. Phone: 08-836-88-4532; Fax: 08-836-88-3844; E-mail: shinji@ed.yama.tus.ac.jp.
‡ Tokyo University of Science.
§ Tohoku University.
|| Present address: Department of Biochemistry, Institute of Development, Aging and Cancer, Tohoku University, Sendai 980-8575, Japan.
⊥ Wayne State University.
University of California.

[1] Abbreviations: BR, bacteriorhodopsin; EPR, electron paramagnetic resonance; UVRR, ultraviolet resonance Raman.

10.1021/bi012190b CCC: $22.00
Published on Web 04/27/2002

C−D loops increased in the M → N transition (*14*). X-ray diffraction of the M_N intermediate of D96N revealed structural disorder of the cytoplasmic end of helix F and the E−F interhelical loop (*15*). Recently, the structure of wild-type BR in the M state has been reported at 2.25 Å resolution by X-ray diffraction, and the crystal structure shows a bend rather than a tilt of the F helix (*16*). In contrast, the outward tilt of helix F has been supported by a recent electron diffraction study on the D96G, F171C, F219L triple mutant, which is locked in the cytoplasmically open state (*17*). The crystallographic structure of the M state of the E204Q mutant had suggested that the tilt is caused by the repacking of side chains between helices F and G, initiated by displacement of the 13-methyl group against Trp182 as the retinal assumed a more relaxed 13-cis configuration (*18*). In this "early" M state already, several additional water molecules appeared near Asp96, probably the beginnings of a hydrogen-bonded chain that later extends to the Schiff base.

Recently, we have found a large decrease in the hydrophobic interaction of the indole ring of a Trp residue in the N intermediate of wild-type BR and assigned it to Trp182 (*19*). Since Trp182 belongs to helix F and is interacting with the retinal polyene chain from the cytoplasmic side (*20*), the decrease in hydrophobic interaction is ascribed to an increase in water permeability in the cytoplasmic half of the protein caused by the tilt of helix F. To study the structural changes around helix F during the photocycle, we have examined the structures and environments of Trp182 and Trp189, which are, respectively, located on the cytoplasmic and extracellular sides of helix F, in the L−N phase by time-resolved UV resonance Raman (UVRR) spectroscopy. The UVRR spectra have revealed structural changes around these Trp residues during the proton transport across the cell membrane.

MATERIALS AND METHODS

Sample Preparation. The W182F and W189F mutants of BR were prepared as described previously (*21, 22*). Purple membranes of wild-type and mutant BR were purified by the standard method (*23*) and suspended at a concentration of 120 μM (for probing at 244 nm) or 20 μM (229 nm probe) in 10 mM HEPES [*N*-(2-hydroxyethyl)piperazine-*N*′-(2-ethanesulfonic acid)] buffer (pH 7.0) or in 10 mM CHES [2-(*N*-cyclohexylamino)ethanesulfonic acid] buffer (pH 9.5) containing 200 mM KCl. Both buffers contained additional 10 (244 nm probe) or 5 mM (229 nm probe) KNO_3, which was used as an internal standard of Raman scattering intensity. All the chemicals used were of the highest grade, and no further purification was attempted.

Time-Resolved UVRR Spectroscopy. Time-resolved UVRR spectra were recorded by using a dual-beam flow apparatus described previously (*19, 24*). The shortest delay time achievable with the apparatus was 20 μs. A line-focused (height, 2 mm; width, 40 μm) visible beam (514.5 nm, 150 mW) from an Ar^+ laser (NEC, GLG-3302) was employed to initiate the photocycle in the sample recirculated by a peristaltic pump from a 30 mL reservoir through a quartz capillary (i.d., 1.5 mm). A UV probe beam (244 or 229 nm, 3 mW) from an intra-cavity frequency-doubled Ar^+ laser (Coherent, Innova 300 FReD) was focused (height, 2 mm; width, 40 μm) downstream from the visible pump beam. The flow velocity and the distance between the pump and probe beams were adjusted to obtain the desired delay time. The temperature of the sample suspension was kept at 16−18 °C during spectral acquisition. Raman scattered light was collected with a quartz lens and introduced to a fore-prism UV Raman spectrometer (*25*) equipped with a liquid nitrogen cooled CCD detector (Princeton Instruments, LN/CCD-1752). Typically, individual Raman spectra were recorded with an accumulation time of 2 h, and difference spectra between the photointermediate and light-adapted BR were computed by using the sums of spectra recorded on 3−4 fresh samples. Wavenumber calibration was effected using the Raman spectrum of a cyclohexanone−acetonitrile mixture (1:1, v/v), and peak wavenumbers were reproducible to within ±1 cm^{-1}.

RESULTS

Time-Resolved 244-nm Raman Spectra. The UVRR spectrum of light-adapted wild-type BR recorded with the 244-nm probe beam is shown in the upper panel of Figure 1. In the lower panel, we show time-resolved difference spectra obtained by subtracting the spectrum of light-adapted (ground state) BR from the spectra recorded at delay times of 20 μs (A), 200 μs (B), and 2 ms (C). During this time frame, the L−M equilibrium shifts in stages toward M, an observation generally interpreted as the formation of several sequential M substates (reviewed in *6*). For simplicity, we consider here only the sequence L−M_1−M_2−N−O. The fractional concentrations of the intermediates at individual delay times are calculated to be L:M_1:M_2:N = 0.70:0.20:0.05:0.00 at 20 μs, 0.30:0.11:0.55:0.02 at 200 μs, and 0.00:0.00:0.65:0.25 at 2 ms by using the reported rate constants of the photocycle (*26*). The fractional concentrations indicate that the difference spectra in traces A, B, and C mainly show changes of the UVRR spectrum on going from the ground state to the L (+M_1), M_2 (+L), and M_2 (+N) intermediates, respectively (the second major component is indicated in parentheses). Accordingly, if a peak is observed only in spectrum A, it may be associated with the M_1 intermediate. Likewise, peaks unique to spectrum C are assigned to the N intermediate. On the other hand, peaks commonly appearing in spectra A and B but not in C are ascribed to L, and those seen only in spectra B and C are assigned to M_2. Most peaks in the UVRR difference spectra in Figure 1 arise from Trp and Tyr side chain vibrations as denoted with labels W and Y, respectively, followed by their mode numbers (*27*). In this paper, we focus on the changes of Trp Raman bands during the photocycle.

Wavenumber shifts and intensity changes are observed for the Trp W3 (∼1550 cm^{-1}), W7 (∼1360 cm^{-1}), W16 (∼1010 cm^{-1}), and W18 (∼760 cm^{-1}) bands. The Trp signals in the UVRR difference spectra in Figure 1 are possibly contributed from eight Trp residues in wild-type BR. To reveal the contribution from a specific Trp residue, mutation of the Trp residue to Phe is useful as demonstrated previously (*28*). This is because the UVRR intensity of Phe is much lower than that of Trp when probed at 244 and 229 nm and the Trp → Phe mutation simply erases the contribution from the mutated Trp residue in the UVRR spectrum. In this study, we have used the W182F and W189F mutants to obtain the UVRR spectra of Trp182 and Trp189, respectively.

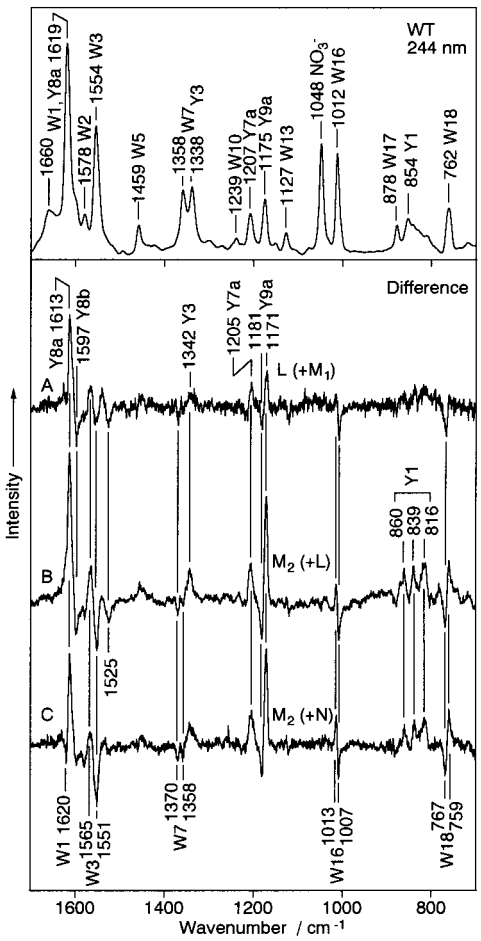

FIGURE 1: Upper panel: 244-nm-probed UVRR spectrum of light-adapted wild-type BR (120 μM) in 10 mM HEPES buffer (pH 7.0) containing 10 mM KNO_3. Lower panel: time-resolved difference spectra recorded at 20 μs (A), 200 μs (B), and 2 ms (C) after photoexcitation with a 515-nm pump beam (150 mW). The difference spectra were obtained by subtracting the 244-nm probe-only spectrum from the pump−probe spectrum by using the 1048-cm^{-1} band of NO_3^- as an internal intensity standard. The power of the probe beam was 3 mW for all the spectra. The Trp and Tyr Raman bands are labeled with W and Y, respectively, followed by the vibrational mode notations (*27*). The band at 1660 cm^{-1} is due to an overlap of the amide I vibration and the C=C stretch of unsaturated lipid.

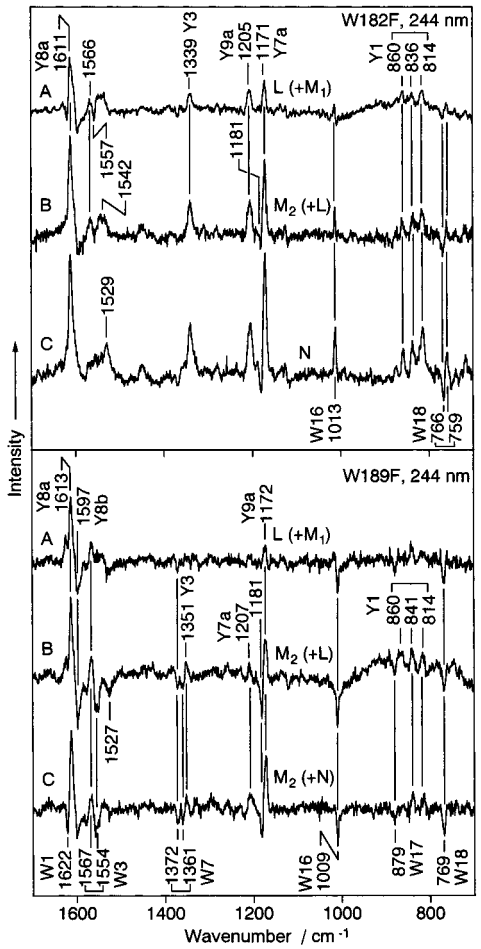

FIGURE 2: Time-resolved UVRR difference spectra (244-nm probe) of W182F (120 μM, upper panel) and W189F (120 μM, lower panel). Delay times: 20 μs (A), 1.5 ms (B), and 15 ms (C) for W182F; 20 μs (A), 200 μs (B), and 2 ms (C) for W189F. The solution conditions and the laser powers are the same as in Figure 1.

Figure 2 shows time-resolved UVRR difference spectra of the W182F (upper panel) and W189F mutants (lower panel) obtained by using the 244-nm probe beam. A transient absorption spectroscopic study on the W182F mutant has shown that the mutation causes a large delay of the L → M transition and the concentrations of M and N intermediates become maximal at around 1.5 and 15 ms, respectively (*29*). Spectrum A of the W182F mutant was therefore recorded at the same delay time (20 μs) as that for the wild type, but the recording of spectra B and C was made at much later time points (1.5 and 15 ms). On the other hand, the M intermediate of the W189F mutant is generated at a rate very similar to that of wild-type BR (*30*), suggesting that the photocycle of the W189F mutant is not much affected by the mutation. Accordingly, the time-resolved UVRR spectra of the W189F mutant were recorded at the same delay times as employed for wild-type BR, i.e., 20 μs (spectrum A), 200 μs (B), and 2 ms (C). Although the lack of kinetic data on the photocycles of the mutants does not permit us to evaluate the fractional concentrations of intermediates at each delay time, difference spectra A, B, and C of the W182F and W189F mutants in Figure 2 are supposed to correspond to difference spectra A, B, and C, respectively, of the wild type in Figure 1. Comparison between the spectra of the wild type and mutants helps us to assign the peaks observed in the time-resolved difference spectra of wild-type BR.

Wild-type BR exhibits a pair of positive (1565 cm^{-1}) and negative (1551 cm^{-1}) peaks in the W3 mode region of the difference spectra (Figure 1). The corresponding peak pair is not seen in the difference spectra of the W182F mutant (Figure 2, upper panel) but is conserved in the spectra of the W189F mutant (Figure 2, lower panel). Therefore, the W3 peak pair of wild-type BR in Figure 1 is ascribed to Trp182. Generally in difference spectra, if a band shifts to a small extent without change in intensity, a derivative-like feature appears with positive and negative peaks of the same height. The heights of the positive and negative peaks of the Trp182 W3 band are comparable in spectra A and B in Figure 1, but the negative peak is larger than the positive one in spectrum C. This observation suggests that the W3 mode of Trp182 shifts to a higher wavenumber in the L−M_2 states and undergoes intensity decrease in the N state.

The 1370-cm^{-1} negative peak in difference spectra A, B, and C of wild-type BR (Figure 1) disappears in the difference

spectra of W182F (Figure 2, upper panel), whereas the W189F difference spectra give a corresponding negative peak at 1372 cm^{-1} (Figure 2, lower panel). The disappearance of the 1370-cm^{-1} negative peak in the W182F spectrum confirms the previous assignment that the 1370-cm^{-1} component of W7 band arises from Trp182 as a result of strong repulsive interaction with the methyl groups of retinal (*28*). The 1370-cm^{-1} component of W7 is characteristic of Trp182 and can be used as a marker of structural change around Trp182 (*28*).

The W16 mode of wild-type BR gives a pair of peaks at 1013 and 1007 cm^{-1} in the difference spectra, though the 1013-cm^{-1} component is prominent only at 200 μs and 2 ms (Figure 1). The W182F mutant, on the other hand, shows only a positive peak at 1013 cm^{-1} without any negative peak around 1007 cm^{-1} (Figure 2, upper panel). Conversely, the W189F mutant exhibits only the lower-wavenumber component at 1009 cm^{-1} (Figure 2, lower panel, traces B and C). These observations indicate that the positive peak at 1013 cm^{-1} of wild-type BR, which disappears in the W189F mutant, is assignable to Trp189 and the negative peak at 1007 cm^{-1}, which disappears in the W182F mutant, is ascribed to Trp182. Since the 1007-cm^{-1} negative peak of wild-type BR is observable at any delay times from 20 μs to 2 ms (A, B, and C in Figure 1), it is concluded that the W16 band intensity of Trp182 is reduced before the formation of the L intermediate. On the other hand, the positive 1013-cm^{-1} peak of wild-type BR is clearly seen only in spectra B and C of Figure 1, suggesting that an intensity increase occurs for the W16 band of Trp189 in the $M_1 \rightarrow M_2$ transition.

In the wavenumber region of the W18 mode, wild-type BR shows a negative peak at 767 cm^{-1} in spectrum A and an additional positive peak at 759 cm^{-1} in spectra B and C (Figure 1). These spectral features are not much affected by the Trp182 → Phe mutation (Figure 2, upper panel), whereas the 759-cm^{-1} positive peak in spectra B and C does not appear in the corresponding difference spectra of the W189F mutant (Figure 2, lower panel). The 759-cm^{-1} band is assigned to the W18 mode of Trp189, which gains intensity in the $M_1 \rightarrow M_2$ transition.

In addition to the prominent peaks described above, a small negative peak is seen at 1620 cm^{-1} in the difference spectrum at 2 ms (Figure 1C). The corresponding peak is absent in the W182F spectrum (Figure 2, upper panel, trace C) but is clearly seen at 1622 cm^{-1} in the W189F spectrum (Figure 2, lower panel, trace C). These observations indicate that the 1620-cm^{-1} negative peak of wild-type BR is due to the W1 mode of Trp182 and its intensity decreases in the N state.

Time-Resolved 229-nm Raman Spectra. In the lower panel of Figure 3, we show UVRR difference spectra of wild-type BR recorded with the 229-nm probe beam at the same delay times as those employed for the 244-nm probe. In the upper panel, the original spectrum of light-adapted BR is shown. In contrast to the spectra probed at 244 nm, negative peaks dominate the 229-nm difference spectra. The wavelength of the 229-nm probe beam is very close to the λ_{max} (~220 nm) of the indole B_b transition, and the intensities of resonance-enhanced Raman bands are strongly influenced by a change in λ_{max} and/or absorption intensity. Figure 4 shows the 229-nm-probed time-resolved difference spectra of the W182F and W189F mutants. The negative peaks observed for the

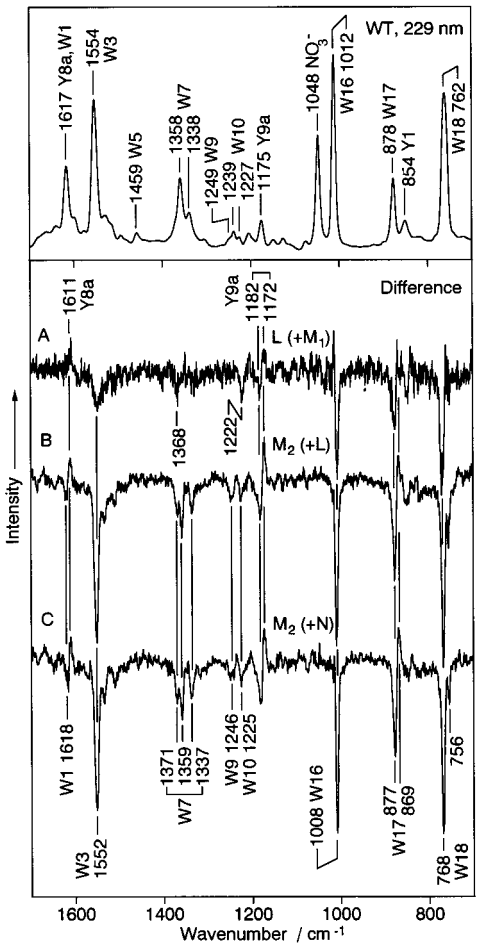

FIGURE 3: Upper panel: 229-nm-probed UVRR spectrum of light-adapted wild-type BR (20 μM) in 10 mM HEPES buffer (pH 7.0) containing 5 mM KNO_3. Lower panel: time-resolved difference spectra recorded at 20 μs (A), 200 μs (B), and 2 ms (C) after photoexcitation with a 515-nm pump beam (150 mW). The difference spectra were obtained by subtracting the 229-nm probe-only spectrum from the pump−probe spectrum by using the 1048-cm^{-1} band of NO_3^- as an internal intensity standard. The power of the probe beam was 3 mW for all the spectra.

wild type become significantly smaller in the W182F mutant when the Tyr signals in the 1185−1170-cm^{-1} region are used as an intensity reference. This observation indicates that Trp182 is mainly responsible for the decrease of 229-nm Raman intensity of wild-type BR. The large intensity decrease may be due to a blue shift and/or an intensity decrease of the B_b transition of Trp182 in the M_1−N phase.

An advantage of using the 229-nm probe is that the Trp W17 mode, which was covered by the Tyr Y1 bands in the 244-nm-probed spectra, is no longer interfered by the Tyr Raman scattering (compare Figures 1 and 3). In spectra B and C of Figure 3, a pair of negative (877 cm^{-1}) and positive (869 cm^{-1}) peaks is clearly seen. The large amplitude of the negative peak compared to that of the positive peak may indicate an overlap of a derivative-like peak pair with purely negative peaks. The peak pair disappears in the spectra of the W182F mutant (Figure 4, upper panel) but is conserved in the spectra of the W189F mutant (Figure 4, lower panel). A wavenumber downshift of the W17 band of Trp182 in the $M_1 \rightarrow M_2$ transition must be the origin of the peak pair. On the other hand, the W17 wavenumber of the Trp189 side chain does not change significantly during the photocycle.

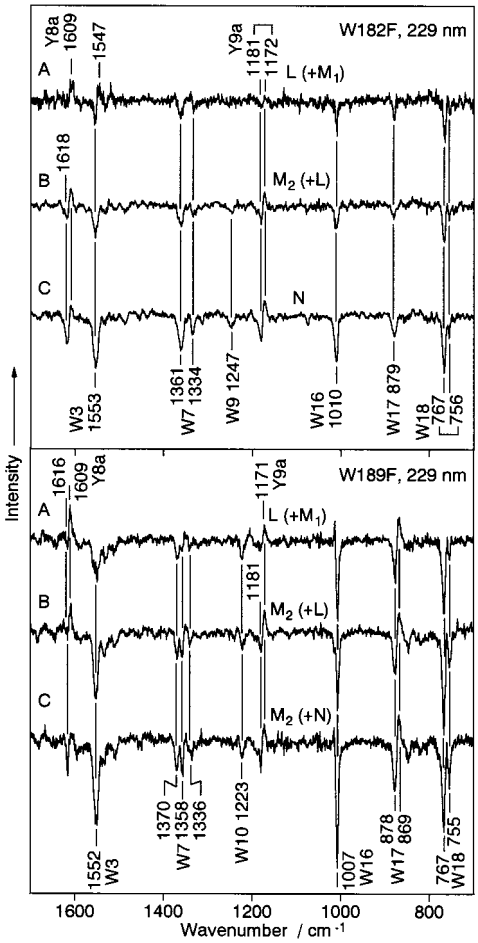

FIGURE 4: Time-resolved UVRR difference spectra (229-nm probe) of W182F (20 μM, upper panel) and W189F (20 μM, lower panel). Delay times: 20 μs (A), 1.5 ms (B), and 15 ms (C) for W182F; 20 μs (A), 200 μs (B), and 2 ms (C) for W189F. The solution conditions and the laser powers are the same as in Figure 3.

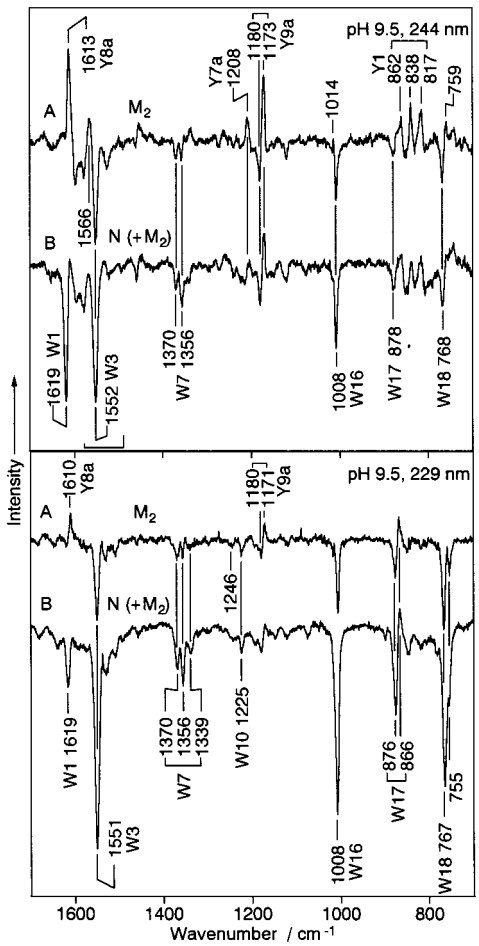

FIGURE 5: Time-resolved UVRR difference spectra of wild-type BR suspended in 10 mM CHES buffer (pH 9.5) containing 200 mM KCl and 5 mM KNO_3. Light-adapted BR was pumped at 515 nm (150 mW) and probed at 244 (3 mW, upper panel) or 229 nm (3 mW, lower panel). The delay times are 100 μs (A) and 10 ms (B) in both panels.

In the 1300−1200-cm^{-1} region of the 229-nm-probed spectra of wild-type BR (Figure 3), new negative peaks are seen at 1246 and 1225 cm^{-1}, which are assignable to the Trp W9 and W10 modes, respectively (*31*). The former peak disappears in the spectra of W189F, and the latter does in the spectra of W182F, indicating that the W9 band of Trp189 and the W10 band of Trp182 both decrease in intensity. The W9 intensity decrease of Trp189 occurs in the $M_1 \rightarrow M_2$ transition because the W9 negative peak shows up only in the spectra at 200 μs and 2 ms (Figure 3B,C). In contrast, the W10 intensity decrease of Trp182 is observed at any delay times of 20 μs, 200 μs, and 2 ms (Figure 3), indicating that the intensity decrease has already occurred in the L intermediate and is maintained in the M and N intermediates. The W10 band of Trp is usually very weak in UVRR spectra (*31, 32*), but the band of Trp182 appears clearly in both 244-nm (*28*) and 229-nm spectra of wild-type BR in the ground state (Figure 3, upper panel). Since the intensity of the W10 band decreases with the decrease of the 1370-cm^{-1} component of W7, a marker of steric repulsion, in the BR → L transition, the unusual intensity of the W10 band of Trp182 may be related to the strong steric repulsion between its indole ring and methyl groups of retinal in the ground state of BR.

UVRR Difference Spectra of the N Intermediate. At neutral pH, the N intermediate of wild-type BR decays rapidly, and its molar fraction rises to no more than 0.3 during the photocycle (*26*). Accordingly, definitive detection of spectral changes characteristic of the N intermediate is difficult at pH 7.0. At alkaline pH, however, the N intermediate accumulates to a significant amount because of delayed recovery of the BR state (*33*−*35*). For example, the N intermediate becomes the major component with molar factions of 0.6 for N and 0.2 for M_2 at 10 ms after photoexcitation in alkaline suspension at pH 9.5, while the M_2 intermediate is predominant at 100 μs under the same conditions (*35*). Figure 5 shows time-resolved UVRR difference spectra of wild-type BR at pH 9.5 probed at 244 (upper panel) and 229 nm (lower panel). The delay times are 100 μs (A) and 10 ms (B) in both panels and spectra A and B are regarded as representing changes on going from the ground state to the M_2 and N (+M_2) states, respectively.

The negative (876 cm^{-1}) and positive (866 cm^{-1}) peak pair in the W17 wavenumber region of the 229-nm-probed spectra (Figure 5, lower panel) well corresponds to the peak pair at 877/869 cm^{-1} observed for the M_2 intermediate (Figure 3B,C) and assigned to Trp182. In addition to the spectral features common to the M_2 and N states, several features characteristic of the N state are also seen. In the 244-nm-probed spectrum of the N (+M_2) state (Figure 5, upper panel, trace B), a new strong negative peak appears

Table 1: Raman Signals of Protein Structural Changes in the L, M_1, M_2, and N Intermediates[a]

residue	mode	ν (cm^{-1})	L	M_1	M_2	N
Trp182	W1	1618				I⇓
	W3	1565/1552 (1552)[b]	ν↑	ν↑	ν↑	I⇓
	W7	1370	I↓	I↓	I↓	I⇓
	W10	1225	I↓	I↓	I↓	I⇓
	W16	1007	I↓	I↓	I↓	I⇓
	W17	877/869 (876/866)[b]			ν↓	ν↓
Trp189	W9	1246			I↓	
	W16	1013			I↑	
	W18	759			I↑	

[a] Changes compared to the light-adapted ground-state (BR). I, intensity; ν, wavenumber; ↑, increase or upshift; ↓, decrease or downshift. [b] Wavenumbers in parentheses are in the N state.

at 1619 cm^{-1}. This negative peak is likely to correspond to the small negative peak at 1620 cm^{-1} detected in the M_2 (+N) spectrum at pH 7.0 and assigned to the W1 mode of Trp182 (Figure 1C). The W1 intensity of Trp182 largely decreases in the $M_2 \rightarrow$ N transition (Figure 5, upper panel). Another difference between the M_2 and N (+M_2) spectra is seen for the W3 mode. The 1566/1552-cm^{-1} peak pair in the M_2 spectrum (Figure 5, upper panel, trace A), which was also observed in the M_2 (+N) spectrum (Figure 1C) and ascribed to an upshift of the W3 mode of Trp182, becomes a single negative peak at 1552 cm^{-1} in the N (+M_2) spectrum (Figure 5, upper panel, trace B). The W3 wavenumber of Trp182 increases in the L−M_2 states but goes back to that of the BR state in the N state with a concomitant intensity decrease. In addition to the spectral differences described above, the negative peaks assigned to the W7, W10, and W16 modes of Trp182 are enhanced upon transition from M_2 to N both in the 244- and in the 229-nm spectra (Figure 5). The UVRR bands of Trp182 generally show a large intensity decrease on going from M_2 to N.

Structural differences around Trp189 between the M_2 and N states are also suggested by the UVRR difference spectra. The positive peaks at 1013 (W16) and 759 cm^{-1} (W18) assigned to Trp189 in the M_2 state (Figure 1B,C) are not seen in the 244-nm-probed N (+M_2) spectrum (Figure 5, lower panel, trace B). The negative peak at 1246 cm^{-1} (W9) of Trp189 in the M_2 state (Figure 3B,C) is not clearly seen either in the 229-nm-probed N (+M_2) spectrum (Figure 5, lower panel, trace B). These positive and negative peaks are the markers of structural changes around Trp189, and their disappearance in the N (+M_2) spectra indicates that the protein structure around Trp189 in the N state is very similar to that in the BR state.

DISCUSSION

The time-resolved UVRR difference spectra of wild-type BR show several features that may be related to protein structural changes near Trp residues during the photocycle. By using the W182F and W189F mutants, most of the Raman signals are assigned to either Trp182 or Trp189 as summarized in Table 1. Among eight Trp residues of BR, Trp182 and Trp189 on helix F are good probes of the structural changes during the photocycle. One of the novel findings of this study is that Raman signals from these Trp residues differ between the M_1 and M_2 intermediates, which enables us to discuss the structural change in the $M_1 \rightarrow M_2$ transition.

Structural Changes in the L−M_2 States. The W7 (1370 cm^{-1}), W10 (1225 cm^{-1}), and W16 (1007 cm^{-1}) modes of Trp182 lose Raman intensity in the L state compared to the BR ground state, and the intensity decrease persists in the M_1 and M_2 states (Table 1). The W7 mode of Trp usually gives a doublet at 1360/1340 cm^{-1} (*36*). The unusual third component at 1370 cm^{-1} of Trp182 arises from a strong steric repulsion between the indole ring of Trp182 and the 9- and 13-methyl groups of retinal as reported previously (*28*). As the intensity decrease of the 1370-cm^{-1} component occurs before formation of L, it is ascribed to a partial reduction of the steric repulsion associated with the retinal isomerization from all-trans to 13-cis in the J → K transition. The reduction of steric repulsion is consistent with the previous observations that the isomerization of retinal accompanies a large displacement of the 13-methyl group (*18*), and that the W28 mode, which is an out-of-plane vibration and has an elevated wavenumber due to the repulsion in the ground state, is shifted to a lower wavenumber in the L intermediate (*29*). The intensity decreases of the W10 mode, which is clearly seen in the UVRR spectrum of Trp182 (*28*), and of the W16 mode may also be ascribed to the reduction of steric repulsion. The wavenumber upshift of the W3 mode (1565/1551 cm^{-1}) is seen for the L, M_1, and M_2 intermediates. The W3 wavenumber is sensitive to the absolute value of the torsion angle, $|\chi^{2,1}|$, about the bond connecting the C_β atom to the indole ring of Trp (*37, 38*). The upshift of the W3 band is therefore ascribed to an increase in $|\chi^{2,1}|$ of Trp182, which occurs in concert with the reduction of steric repulsion. Yamazaki et al. have reported that the hydrogen bond of Trp182 becomes very weak specifically in the L intermediate, on the basis of an infrared band at 3486 cm^{-1} (*30*). However, we cannot detect any change of the W17 band (a hydrogen bond marker, vide infra) in our L (+M_1) UVRR spectra. The weakening of the Trp182 hydrogen bond might occur in an early stage of L formation.

In addition to the changes described above, a wavenumber downshift was observed for the W17 mode in the $M_1 \rightarrow M_2$ transition (Table 1). It is known that the W17 mode decreases in wavenumber with increase of the strength of hydrogen bonding at the indole nitrogen (*39*). The wavenumber downshift, therefore, indicates an increase in hydrogen bonding strength of the Trp182 indole ring in the $M_1 \rightarrow M_2$ transition. In a previous study, we showed that the Trp182 indole ring of BR was hydrogen bonded to a water molecule buried in an adjacent hydrophobic cavity (*28*), which was later confirmed by X-ray diffraction (*20, 40*). Generally, the UVRR bands of Trp are enhanced in resonance with the B_b transition (*32, 41*), and their UVRR intensities increase with increase in hydrogen bonding strength or in hydrophobic interaction (*31*). The increase of hydrogen bonding strength of Trp182 predicts an increase in UVRR intensity in the $M_1 \rightarrow M_2$ transition, though the actual intensity does not much differ from those in the L and M_1 states. This observation can be explained by assuming that the hydrophobic interaction of Trp182 decreases in the $M_1 \rightarrow M_2$ transition and compensates the intensity increase associated with the change in hydrogen bonding.

According to the atomic model of ground-state BR (*20*), a water molecule (Wat501) bridges Trp182 on helix F and the amide C=O of Ala215 on helix G through interhelical hydrogen bonding. The hydrogen bond of the water molecule

with Ala215 C═O is disrupted, and a new hydrogen bond is formed with the hydroxyl group of Thr178 in the wild-type M-state model (*16*, Wat501 in the ground-state model corresponds to Wat721 in the M-state model). Similar structural changes have been reported for the M intermediates of the E204Q (*18*) and D96N mutants (*15*). Since Trp182 and Thr178 are located on the same side of helix F and the water molecules are readily accessible to both Trp182 and Thr178, the hydrogen bonding between the water and Trp182 in the Trp182−water−Thr178 bridge of the M-state model may be stronger than that in the interhelical Trp182−water−Ala215 bridge of the ground-state model. This is consistent with the UVRR finding that the hydrogen bond of Trp182 is strengthened in the M_2 state. The M-state model of wild-type BR also exhibits an additional water molecule, Wat722, between Wat721 and Ala215. The presence of Wat722 possibly indicates an increase in water accessibility in this region associated with a decrease in the hydrophobic interaction of Trp182 in the M_2 intermediate as suggested by the present UVRR study. The increased water accessibility in this region probably contributes to a proton transfer from Asp96 to the Schiff base in the $M_2 \rightarrow N$ step of the photocycle. The present UVRR difference spectra show that steric conflict between the indole ring of Trp182 and retinal is partly resolved in the L state but the disruption of the interhelical hydrogen bond associated with a relocation of water molecules takes place in the $M_1 \rightarrow M_2$ transition.

The 244-nm UVRR intensities of the W16 (1013 cm^{-1}) and W18 (759 cm^{-1}) bands of Trp189 increase only in the M_2 state (Figure 1, Table 1). This observation indicates that the protein structure around Trp189 is significantly affected neither by the retinal isomerization in the $J \rightarrow K$ transition nor by deprotonation of the Schiff base in the $L \rightarrow M_1$ transition. Since the W16 and W18 bands of Trp are enhanced in resonance with the B_b transition (*32*, *41*), the intensity increases of these bands can be explained by a red-shift of the B_b absorption maximum of Trp189 in the M_2 state. In contrast, the 229-nm-probed spectra show an intensity decrease of the W18 (756 cm^{-1}) band of Trp189 (Figures 3 and 4). We have shown that the B_b transition of Trp189 is already red-shifted in the BR state (*28*). If the λ_{max} of the B_b transition of Trp189 further shifts to a wavelength longer than 229 nm but shorter than 244 nm in the M_2 intermediate, the Raman bands would show intensity decreases in the 229-nm-probed spectra and increases in the 244-nm-probed spectra. A largely red-shifted excitation profile ($\lambda_{max} = 230$ nm) has been reported for single Trp residue in horse-heart cytochrome *c* (*42*). A similar red-shift is likely to occur for Trp189 in the M_2 state. The B_b transition undergoes a red-shift when the strength of hydrogen bonding at the indole nitrogen or hydrophobic interaction of the indole ring with the environment increases (*31*). The 229-nm UVRR difference spectra have shown that the W17 wavenumber, which is sensitive to the hydrogen bonding, does not change for Trp189. Therefore, the intensity increases of W16 and W18 in the 244-nm difference spectrum are ascribed to a red-shift of the B_b transition caused by an increase in hydrophobic interaction of Trp189 in the $M_1 \rightarrow M_2$ transition.

The indole ring of Trp189 faces the β-ionone ring of retinal and is buried in a hydrophobic cavity formed by the side chains of Ala126 (helix D), Trp138 (E), Phe135 (E), Leu190 (F), Phe208 (G), and Glu194 (F−G loop) (*20*). In addition, the indole nitrogen of Trp189 is hydrogen bonded to the phenolic oxygen of Tyr83 on helix C. The M-state model of wild-type BR shows that the indole ring is displaced toward the extracellular side with little change in hydrogen bonding between Trp189 and Tyr83 (*16*). The persistence of hydrogen bonding is consistent with our UVRR observation, and the increased hydrophobic interaction of Trp189 may be a consequence of an increased interaction with the β-ionone ring associated with the tilt of helix F. Since the Trp189 indole ring is in contact with the methylene group of the Glu194 side chain, it is possible that the environmental change of Trp189 is partly due to a change in interaction with the side chain of Glu194, which plays a key role in releasing a proton to the extracellular medium in the $M_1 \rightarrow M_2$ transition and may be affected by the resultant redistribution of the electrical charge.

A large outward tilt of helix F from the center of the protein was proposed by electron and X-ray diffraction studies of the M and N intermediates (*9*, *11*−*13*). A recent electron diffraction study on a triple mutant in the open structure has supported the outward tilt of helix F (*17*), while the M-state model of wild-type BR obtained by X-ray diffraction shows a bend of helix F with an outward tilt of the cytoplasmic half of the helix (*16*). A kinetic analysis of transient EPR and visible absorption spectra has revealed that the outward tilt of helix F occurs during the lifetime of the M intermediate (*43*). In this study, we have found that the hydrophobic interaction of Trp189 is significantly increased in the M_2 state. The environmental change of Trp189 probably indicates that the outward tilt of helix F starts in the $M_1 \rightarrow M_2$ transition.

Structural Changes in the M_2−N Phase. One of the major events during the $M_2 \rightarrow N$ transition is the proton transfer from Asp96 to the Schiff base. The proton transfer is considered to be promoted by lowering the pK_a of Asp96, which has an unusually high pK_a in the hydrophobic environment of ground-state BR (*44*, *45*). It is interesting to discuss the relationship between the tilt of helix F and the reprotonation of the Schiff base on the basis of the present UVRR findings. The hydrogen bonding state of Trp182 does not change on going from the M_2 to N state because the downshift of the W17 mode of Trp182 in the M_2 state is maintained in the N state (Table 1). In contrast, the W3, W7, and W16 modes of Trp182 exhibit large intensity decreases in the $M_2 \rightarrow N$ transition (Table 1). The intensity decreases are attributed to a large change of the Trp182 environment from hydrophobic to hydrophilic. The environmental change may also affect the B_a transition, which is located at a shorter wavelength than the B_b transition and is the origin of the UVRR intensity of the W1 mode (*32*, *41*). Actually, the W1 mode shows a large intensity decrease in the $M_2 \rightarrow N$ transition (Table 1). The opening of the cytoplasmic side initiated by the tilt of helix F in the $M_1 \rightarrow M_2$ transition is probably completed by a further conformational change around helix F and a rearrangement of interhelical loops on the cytoplasmic side in the $M_2 \rightarrow N$ transition (*14*). The large decrease in the hydrophobic interaction of Trp182 in the $M_2 \rightarrow N$ transition is consistent with an entry of water molecules that may constitute a proton-conducting pathway from the cytoplasmic surface to Asp96 and to the Schiff base. Increased hydration is likely to promote deprotonation of Asp96 and protonation of the

Schiff base. It is also noted that the side chain conformation of Trp182 becomes similar to that of ground-state BR as monitored with the W3 wavenumber (Table 1). In contrast to the development of structural changes on the cytoplasmic side on going from M_2 to N, the structural tension caused by the $M_1 \rightarrow M_2$ transition may be reduced on the extracellular side because the hydrophobic interaction of Trp189 returns to that in the M_1 intermediate as demonstrated by the UVRR intensity (Table 1).

In summary, the dynamic structural and environmental changes around two Trp residues located on the cytoplasmic and extracellular halves of helix F have been examined by time-resolved UVRR spectroscopy under physiological conditions. In the $M_1 \rightarrow M_2$ transition, the strength of hydrogen bonding at the indole nitrogen of Trp182 on the cytoplasmic side increases with a concomitant decrease in hydrophobic interaction. The structural change around Trp182 is consistent with the M-state model of wild-type BR, which shows disruption of the water-mediated interhelical hydrogen bond bridge and relocation of water molecules on the cytoplasmic side of retinal. Concomitant with the change on the cytoplasmic side, hydrophobic interaction of Trp189 on the extracellular side increases transiently. These structural changes suggest that the tilt of helix F occurs in the $M_1 \rightarrow M_2$ transition. In the $M_2 \rightarrow N$ transition, on the other hand, a large decrease in hydrophobic interaction take places for Trp182, indicating that the channel created by the tilt of helix F allows entry of water molecules even to the vicinity of Trp182. Concomitantly, the environment of Trp189 returns to the initial state. The large increase in water permeability on the cytoplasmic side associated with the $M_2 \rightarrow N$ transition is probably correlated with the structural changes in the E−F loop regions on the cytoplasmic surface. Although the switch for reprotonation of the Schiff base is turned on in the $M_1 \rightarrow M_2$ transition with the tilt of helix F, subsequent structural reorganization of the E−F loop regions in the $M_2 \rightarrow N$ transition may be essential for the entry of water molecules into the hydrophobic channel on the cytoplasmic side of BR.

REFERENCES

1. Oesterhelt, D., and Stoeckenius, W. (1973) Functions of a new photoreceptor membrane. *Proc. Natl. Acad. Sci. U.S.A. 70*, 2853−2857.
2. Henderson, R., Baldwin, J., Ceska, T. A., Zemlin, F., Beckmann, E., and Downing, K. H. (1990) Model for the structure of bacteriorhodopsin based on high-resolution electron cryomicroscopy. *J. Mol. Biol. 213*, 899−929.
3. Lozier, R. H., Bogomolni, R. A., and Stoeckenius, W. (1975) Bacteriorhodopsin: a light-driven proton pump in *Halobacterium halobium*. *Biophys. J. 15*, 955−962.
4. Smith, S. O., Courtin, J., and Mathies, R. A. (1985) Determination of retinal chromophore structure in bacteriorhodopsin with resonance Raman spectroscopy. *J. Membr. Biol. 85*, 95−109.
5. Haupts, U., Tittor, J., and Oesterhelt, D. (1999) Closing in on bacteriorhodopsin: progress in understanding the molecule. *Annu. Rev. Biophys. Biomol. Struct. 28*, 367−399.
6. Lanyi, J. K. (2000) Molecular mechanism of ion transport in bacteriorhodopsin: insights from crystallographic, spectroscopic, kinetic, and mutational studies. *J. Phys. Chem. 104*, 1441−1148.
7. Haupts, U., Tittor, J., Bamberg, E., and Oesterhelt, D. (1997) General concept for ion translocation by halobacterial retinal proteins: the isomerization/switch/transfer (IST) model. *Biochemistry 36*, 2−7.
8. Brown, L. S., Dioumaev, A. K., Needleman, R., and Lanyi, J. K. (1998) Local-access model for proton transfer in bacteriorhodopsin. *Biochemistry 37*, 3982−3993.
9. Subramaniam, S., Gerstein, M., Oesterhelt, D., and Henderson, R. (1993) Electron diffraction analysis of structural changes in the photocycle of bacteriorhodopsin. *EMBO J. 12*, 1−8.
10. Sasaki, J., Shichida, Y., Lanyi, J. K., and Maeda, A. (1992) Protein changes associated with reprotonation of the Schiff base in the photocycle of Asp96→Asn bacteriorhodopsin. The MN intermediate with unprotonated Schiff base but N-like protein structure. *J. Biol. Chem. 267*, 20782−20786.
11. Vonck, J. (1996) A three-dimensional difference map of the N intermediate in the bacteriorhodopsin photocycle: part of the F helix tilts in the M to N transition. *Biochemistry 35*, 5870−5878.
12. Vonck, J. (2000) Structure of the bacteriorhodopsin mutant F219L N intermediate revealed by electron crystallography. *EMBO J. 19*, 2152−2160.
13. Kamikubo, H., Kataoka, M., Váró, G., Oka, T., Tokunaga, F., Needleman, R., and Lanyi, J. K. (1996) Structure of the N intermediate of bacteriorhodopsin revealed by X-ray diffraction. *Proc. Natl. Acad. Sci. U.S.A. 93*, 1386−1390.
14. Thorgeirsson, T. E., Xiao, W., Brown, L. S., Needleman, R., Lanyi, J. K., and Shin, Y.-K. (1997) Transient channel-opening in bacteriorhodopsin: an EPR study. *J. Mol. Biol. 273*, 951−957.
15. Luecke, H., Schobert, B., Richter, H.-T., Cartailler, J.-H., and Lanyi, J. K. (1999) Structural changes in bacteriorhodopsin during ion transport at 2 angstrom resolution. *Science 286*, 255−261.
16. Sass, H. J., Büldt, G., Gessenich, R., Hehn, D., Neff, D., Schlesinger, R., Berendzen, J., and Ormos, P. (2000) Structural alterations for proton translocation in the M state of wild-type bacteriorhodopsin. *Nature 406*, 649−653.
17. Subramaniam, S., and Henderson, R. (2000) Molecular mechanism of vectorial proton translocation by bacteriorhodopsin. *Nature 406*, 653−657.
18. Luecke, H., Schobert, B., Cartailler, J.-H., Richter, H.-T., Rosengarth, A., Needleman, R., and Lanyi, J. K. (2000) Coupling photoisomerization of retinal to directional transport in bacteriorhodopsin. *J. Mol. Biol. 300*, 1237−1255.
19. Hashimoto, S., Sasaki, M., and Takeuchi, H. (1998) Ultraviolet resonance Raman evidence for the opening of a water-permeable channel in the M to N transition of bacteriorhodopsin. *J. Am. Chem. Soc. 120*, 443−444.
20. Luecke, H., Schobert, B., Richter, H.-T., Cartailler, J.-H., and Lanyi, J. K. (1999) Structure of bacteriorhodopsin at 1.55 Å resolution. *J. Mol. Biol. 291*, 899−911.
21. Ni, B., Chang, M., Duschl, A., Lanyi, J. K., and Needleman, R. (1990) An efficient system for the synthesis of bacteriorhodopsin in *Halobacterium halobium*. *Gene 90*, 169−172.
22. Needleman, R., Chang, M., Ni, B., Váró, G., Fornés, J., White, S. H., and Lanyi, J. K. (1991) Properties of Asp212→Asn bacteriorhodopsin suggest that Asp212 and Asp85 both participate in a counterion and proton acceptor complex near the Schiff base. *J. Biol. Chem. 266*, 11478−11484.
23. Oersterhelt, D., and Stoeckenius, W. (1974) Isolation of the cell membrane of *Halobacterium halobium* and its fractionation into red and purple membrane. *Methods Enzymol. 31*, 667−678.
24. Ames, J. B., Ros, M., Raap, J., Lugtenburg, J., and Mathies, R. A. (1992) Time-resolved ultraviolet resonance Raman studies of protein structure: application to bacteriorhodopsin. *Biochemistry 31*, 5328−5334.
25. Hashimoto, S., Ikeda, T., Takeuchi, H., and Harada, I. (1993) Utilization of a prism monochromator as a sharp-cut bandpass filter in ultraviolet Raman spectroscopy. *Appl. Spectrosc. 47*, 1283−1285.
26. Váró, G., and Lanyi, J. K. (1991) Kinetic and spectroscopic evidence for an irreversible step between deprotonation and

reprotonation of the Schiff base in the bacteriorhodopsin photocycle. *Biochemistry 30*, 5008−5015.
27. Harada, I., and Takeuchi, H. (1986) Raman and ultraviolet resonance Raman spectra of proteins and related compounds. in *Spectroscopy of Biological Systems* (Clark, R. J. H., and Hester, R. E., Eds.) pp 113−175, John Wiley & Sons, New York.
28. Hashimoto, S., Obata, K., Takeuchi, H., Needleman, R., and Lanyi, J. K. (1997) Ultraviolet resonance Raman spectra of Trp-182 and Trp-189 in bacteriorhodopsin: novel information on the structure of Trp-182 and its steric interaction with retinal. *Biochemistry 36*, 11583−11590.
29. Weidlich, O., Schalt, B., Friedman, N., Sheves, M., Lanyi, J. K., Brown, L. S., and Siebert, F. (1996) Steric interaction between the 9-methyl group of the retinal and tryptophan 182 controls 13-cis to all-trans reisomerization and proton uptake in the bacteriorhodopsin photocycle. *Biochemistry 35*, 10807−10814.
30. Yamazaki, Y., Sasaki, J., Hatanaka, M., Kandori, H., Maeda, A., Needleman, R., Shinada, T., Yoshihara, K., Brown, L. S., and Lanyi, J. K. (1995) Interaction of tryptophan-182 with the retinal 9-methyl group in the L intermediate of bacteriorhodopsin. *Biochemistry 34*, 577−582.
31. Matsuno, M., and Takeuchi, H. (1998) Effects of hydrogen bonding and hydrophobic interactions on the ultraviolet resonance Raman intensities of indole ring vibrations. *Bull. Chem. Soc. Jpn. 71*, 851−857.
32. Su, C., Wang, Y., and Spiro, T. G. (1990) Saturation effect on ultraviolet resonance Raman intensities: excimer/YAG laser comparison and aromatic amino acid cross-sections. *J. Raman Spectrosc. 21*, 435−440.
33. Kouyama, T., Nasuda-Kouyama, A., Ikegami, A., Mathew, M. K., and Stoeckenius, W. (1988) Bacteriorhodopsin photoreaction: identification of a long-lived intermediate N (P, R_{350}) at high pH and its M-like photoproduct. *Biochemistry 27*, 5855−5863.
34. Ames, J. B., and Mathies, R. A. (1990) The role of back-reactions and proton uptake during the N → O transition in bacteriorhodopsin's photocycle: a kinetic resonance Raman study. *Biochemistry 29*, 7181−7190.
35. Váró, G., and Lanyi, J. K. (1990) Pathways of the rise and decay of the M photointermediate(s) of bacteriorhodopsin. *Biochemistry 29*, 2241−2250.
36. Harada, I., Miura, T., and Takeuchi, H. (1986) Origin of the doublet at 1360 and 1340 cm^{-1} in the Raman spectra of tryptophan and related compounds. *Spectrochim. Acta, Part A 42A*, 307−312.
37. Miura, T., Takeuchi, H., and Harada, I. (1989) Tryptophan Raman bands sensitive to hydrogen bonding and side-chain conformation. *J. Raman Spectrosc. 20*, 667−671.
38. Maruyama, T., and Takeuchi, H. (1995) Effects of hydrogen bonding and side-chain conformation on the Raman bands of tryptophan-2,4,5,6,7-d_5. *J. Raman Spectrosc. 26*, 319−324.
39. Miura, T., Takeuchi, H., and Harada, I. (1988) Characterization of individual tryptophan side chains in proteins using Raman spectroscopy and hydrogen−deuterium exchange kinetics. *Biochemistry 27*, 88−94.
40. Pebay-Peyroula, E., Rummel, G., Rosenbusch, J. P., and Landau, E. M. (1997) X-ray structure of bacteriorhodopsin at 2.5 angstroms from microcrystals grown in lipidic cubic phases. *Science 277*, 1676−1681.
41. Sweeney, J. A., and Asher, S. A. (1990) Tryptophan UV resonance Raman excitation profiles. *J. Phys. Chem. 94*, 4784−4791.
42. Liu, G., Grygon, C. A., and Spiro, T. G. (1989) Ionic strength dependence of cytochrome *c* structure and Trp-59 H/D exchange from ultraviolet resonance Raman spectroscopy. *Biochemistry 28*, 5046−5050.
43. Radzwill, N., Gerwert, K., and Steinhoff, H.-J. (2001) Time-resolved detection of transient movement of helices F and G in doubly spin-labeled bacteriorhodopsin. *Biophys. J. 80*, 2856−2866.
44. Gerwert, K., Hess, B., Soppa, J., and Oesterhelt, D. (1989) Role of aspartate-96 in proton translocation by bacteriorhodopsin. *Proc. Natl. Acad. Sci. U.S.A. 86*, 4943−4947.
45. Száraz, S., Oesterhelt, D., and Ormos, P. (1994) pH-induced structural changes in bacteriorhodopsin studied by Fourier transform infrared spectroscopy. *Biophys. J. 67*, 1706−1712.

BI012190B